J Mater Sci (2008) 43:6527–6530
DOI 10.1007/s10853-008-2852-2

The structural and optical properties of ZnO nanorods via citric acid-assisted annealing route

Zao Yang · Quan-Hui Liu

Received: 10 January 2008 / Accepted: 1 July 2008 / Published online: 27 July 2008

Abstract ZnO nanorods with diameters ranging from 25 to 88 nm and with length up to 1 μm were obtained via citric acid-assisted annealing route. The sample was characterized by X-ray diffraction, field-emission scanning electron microscopy (FE-SEM), Raman spectrometer, FTIR spectrophotometer, ultraviolet visible (UV–VIS) spectroscopy, and photoluminescence (PL) spectroscopy. It demonstrates that the sample is composed of ZnO with hexagonal structure and the ZnO nanorods are of excellent optical quality.

Introduction

One-dimensional (1D) nanostructures have been extensively studied due to their potentials as the building blocks for fabricating nanometer-scaled electronic, optoelectronic, electrochemical, and sensor devices. Among the wide variety of 1D semiconductor nanostructures, ZnO is a direct-band-gap semiconductor with an energy gap of 3.3 eV at room temperature. It has higher exciton binding energy (60 meV for ZnO vs. 28 meV for GaN) and higher optical gain (300 cm^{-1}) than GaN (100 cm^{-1}) at room temperature [1]. The optical properties of ZnO, studied using photoluminescence, photoconductivity, and absorption, reflect the intrinsic direct band gap, a strongly bound exciton state, and gap states due to point defects [2]. The photoluminescence (PL) spectra of ZnO usually exhibit ultraviolet (UV) and visible bands. The UV band was identified in terms of free and bound exciton complexes and the phonon replicas [3]. The visible emission is mainly related to deep-level emissions introduced by some defects, such as oxygen vacancies (V_o), Zinc vacancies (V_{Zn}), Zinc interstitials (Zn_i), and anti-site of O_{Zn} [4]. In this paper, ZnO nanorods have been synthesized by citric acid-assisted annealing process. The structural and optical properties were analyzed.

Z. Yang (✉)
College of Materials Science and Engineering,
Hunan University, Changsha 410082, China
e-mail: yangzao888@tom.com

Q.-H. Liu
College of Physics and Microelectronical Science,
Hunan University, Changsha 410082, China

Experimental section

All the chemicals used in this study were of analytical grade and used without farther purification. Four chemicals were needed and they were analytically pure zinc acetate ($Zn(CH_3COO)_2 \cdot 2H_2O$), citric acid ($C_6H_8O_7 \cdot H_2O$), pure distilled water (H_2O) and absolute ethanol (CH_3CH_2OH). In a typical procedure, a solution of citric acid (0.048 M) in ethanol was added to $Zn(CH_3COO)_2$ solutions (1 M) in distilled water. After the addition was finished, the solution (PH value was equal to 6.5) was stirred at 80 °C for 10 h to get the precursor. The precursor was calcined in a muffle furnace for 2 h at 400 °C. Finally, the sample was obtained after cooling down at room temperature in air.

The samples were characterized by powder X-ray diffraction (XRD) using D5000 X-ray diffractometer (SIEMENS, Germany) with Cu monochromatized K_α ($\lambda = 1.5478$ Å) radiation. XRD patterns were recorded from 10° to 80° (2θ) with a scanning step of 0.01°. The size distribution and morphology of the sample were analyzed by field-emission scanning electron microscopy (FE-SEM) (JE0L JSM-6700).The Raman spectra were recorded on a Jobin Yvon

Labram-010 Raman spectrometer with a 514.5-nm Ar^+ laser as excitation source. Infrared (IR) absorption spectroscopy (Nicolet Nexus 870) was carried out at room temperature in the range of 400–4000 cm^{-1} by the FTIR spectrophotometer. UV–visible absorption spectra were recorded using a TU-1900 UV–vis double-beam spectrophotometer. The scanning wavelength range was 300–800 nm. The PL spectrum was recorded using a Hitachi F-4500 fluorescence spectrophotometer.

Results and discussion

Figure 1 shows the XRD patterns of the sample. All the diffraction peaks are quite similar to that of a bulk ZnO, which has a hexagonal spiauterite structure ($a = 3.249$ Å, $c = 5.206$ Å, space group: $P6_3mc$ (186)) and diffraction data are in agreement with JCPDS card of ZnO (JCPDS 36-1451). No characteristic peaks of impurities, such as $Zn(CH_3COO)_2 \cdot 2H_2O$ and other precursor compounds, are observed. Figure 2 shows the typical FE-SEM image of the nanorods. As seen from the figure, the results reveal that ZnO nanorods are straight with diameters ranging from 25 to 88 nm and with length up to 1 μm. The aspect ratio is 10:40.

Raman spectra of the as-made ZnO nanorods measured with the 514.5 nm line of an Ar^+ laser as the excitation source are illustrated in Fig. 3. The Raman spectra are sensitive to crystallization, structural disorder, and defects in micro- and nanostructures. Single-crystalline ZnO has eight sets of optical phonons near the center of the Brillouin Zone, which can be classified as $\Gamma = A_1 + 2B_1 + E_1 + 2E_2$. Among these, A_1, E_1, and E_2 are Raman-active whereas B_1 is forbidden. Moreover, the A_1 and E_1 are polar, and split into two transverse optical (TO) and longitudinal optical (LO) phonons [5]. As shown in Fig. 3, the presence of a sharp and

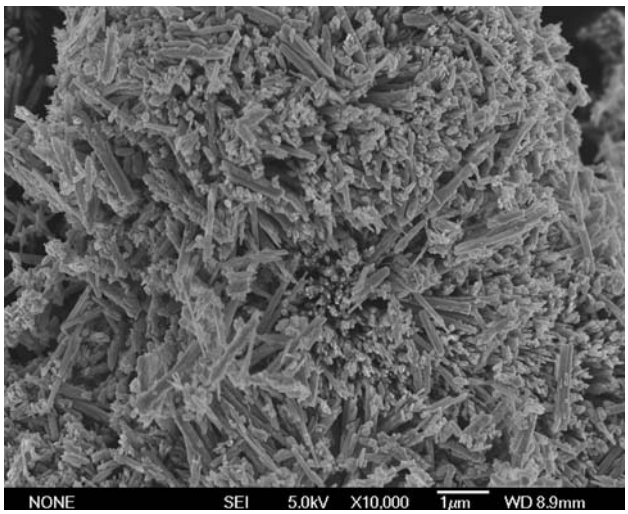

Fig. 2 FE-SEM image of ZnO nanorods

strong nonpolar optical phonon E_2 mode at 431 cm^{-1} confirms that the products formed are wurtzite hexagonal ZnO [6]. Two very small peaks at 325 and 376 cm^{-1} were also obtained which were assigned as E_{2H}–E_{2L} (multi-phonon) and A_{1T} modes, respectively [7]. The peak at 575 cm^{-1} due to the structural defects is attributed to ZnO E_1 (LO) mode, indicating that the grown nanorods having very few or no structural defects [8]. Clearly, it also demonstrates that the sample is composed of ZnO with hexagonal structure.

The sample was mixed with potassium bromide in the ratio of 1:100. The background spectrum recorded using KBr was subtracted from the sample spectrum. Figure 4 exhibits IR spectra for the as-obtained ZnO nanorods, In the IR spectra, ZnO usually shows distinct absorption bands around wave numbers of 464 cm^{-1} [9]. The position and number of these bands not only depend on crystal structure and chemical composition, but also on particle morphology [10]. Studies concerned with this morphology

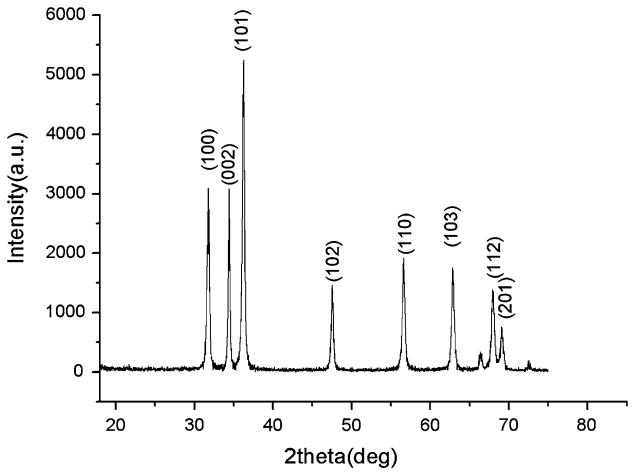

Fig. 1 XRD pattern of ZnO nanorods

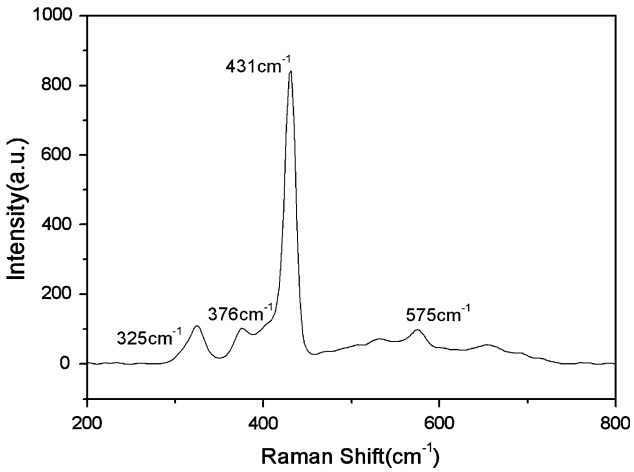

Fig. 3 Raman spectra of the as-prepared ZnO nanorods

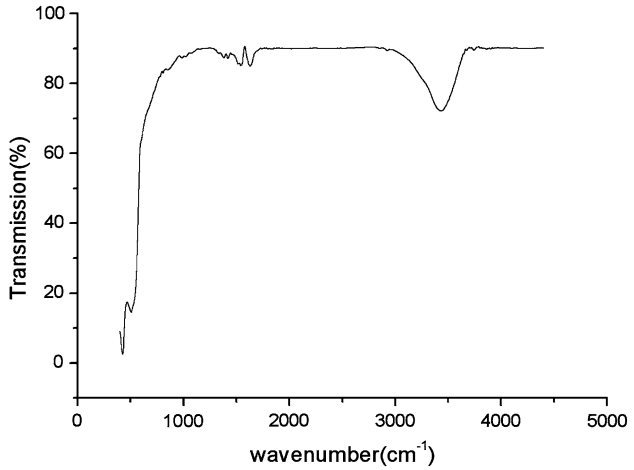

Fig. 4 FTIR spectra of ZnO nanorods

dependency have shown that in case of spherical ZnO particles, calculated as well as measured spectra show one distinct absorption maximum at around 464 cm^{-1} [9]. Since the particle morphology from our syntheses is always nearby spherical, IR measurements resulted always in spectra showing one distinct peak. This maximum broadens and splits into two maxima if the particle morphology changes from spherical to a needlelike shape. The latter is the preferred morphology from wet chemical synthesis routes under certain conditions and is the result of a preferred *c*-axis growth [9]. Therefore, reference spectra of ZnO powders often show two absorption maxima at around 512 and 406 cm^{-1} [11]. In Fig. 3, the spectra show a characteristic ZnO absorption at $\sim$509 cm^{-1}, red-shifted at 512 cm^{-1}. And there will be another characteristic ZnO absorption at 428 cm^{-1}. The frequency 428 cm^{-1} indicates a blueshift of 22 cm^{-1} from 406 cm^{-1}. The broad absorption in $\sim$3433 and $\sim$1630 cm^{-1} are assigned to the existence of hydroxyl groups on the surface of the sample.

The UV–vis absorption spectra of the ZnO nanorods at room temperature are shown in Fig. 5. The absorption spectra have a narrow peak near the band edge in the exciton absorption region (at about 376 nm) and blue-shifted relative to the bulk exciton absorption (380 nm). The stronger exciton effect is an important character of quantum confinement effect in nano-semiconductors, the reason being the carriers are confined in a very small district that makes the electron and hole move only in a potential well. At the same time, it can enhance the coupling interaction with each other. Then, the exciton bounded stronger and probability of binding increased, so we can observe a more apparent exciton absorption peak when the particles' size decreased and hence the blueshift. The dependence of particle size on the optical absorption energy can been expressed based on an effective mass approximation as following equation:

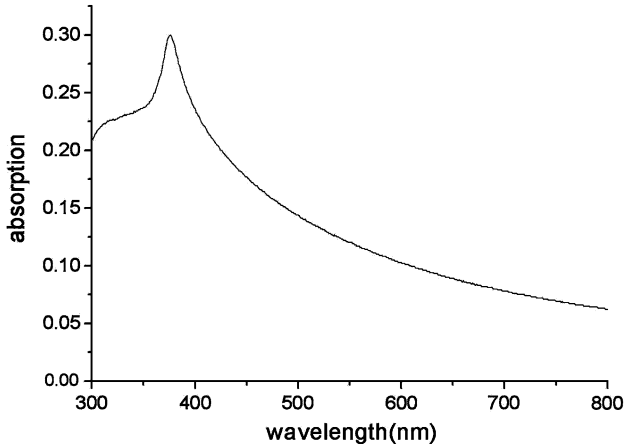

Fig. 5 UV–Vis absorption spectra of ZnO nanorods

$$E_g = E_{g0} + \frac{\hbar^2\pi^2}{2d^2}\left(\frac{1}{m_e} + \frac{1}{m_h}\right) - \frac{1.8e^2}{\varepsilon d}$$

where the cluster and bulk-state band gap energies are E_g and E_{g0}, m_e and m_h are the effective masses of an electron and a hole, respectively. Here ε is the dielectric constant of a semiconductor and d is the average particle size.

Figure 6 shows a room temperature PL spectrum of the obtained ZnO nanorods with 325 nm line of a Xe lamp. The PL spectrum exhibits an intense UV band around 398 nm. The UV emission band must be explained by a near band-edge transition of wide band gap ZnO nanorods, namely the free excitons recombination through an exciton–exciton collision process [12]. Some weak deep-level or trap-state emissions are also seen in the visible spectral region, indicating a small amount of structural defects, such as oxygen vacancies and impurities, exist in the ZnO nanorods [13]. The weaker green light emission of ZnO nanorods might be related to a very low level of oxygen

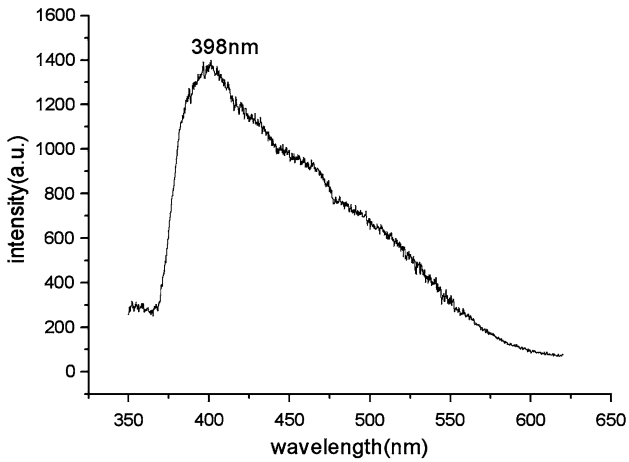

Fig. 6 PL spectrum of ZnO nanorods at room temperature

vacancies. It indicates that the ZnO nanords are of excellent optical quality.

Conclusions

ZnO nanorods with diameters ranging from 25 to 88 nm and with length up to 1 μm were obtained via citric acid-assisted annealing route. From the results of XRD, SEM, Raman, FTIR together with the strong UV emission in the PL spectrum, we can find that the obtained ZnO nanorods have good crystal quality and excellent optical properties when the near band-edge emissions are concerned.

References

1. Wong EM, Searson PC (1999) Appl Phys Lett 74:2939
2. Bethke S, Pan H, Wessels BW (1988) Appl Phys Lett 52:138
3. Studenikin SA, Cocivera M, Kellner W, Pascher H (2000) J Lumin 91:223
4. Chen YF, Bagnall DM, Koh HJ, Park KT, Hiraga K, Zhu ZO, Yao T (1998) J Appl Phys 84:3912
5. Calleja JM, Cardona M (1977) Phys Rev B 16:3753
6. Wu JJ, Liu SC (2002) J Phys Chem B 106:9546
7. Wu JJ, Liu SC (2002) Adv Mater 14:215
8. Umar A, Hahn YB (2006) Appl Phys Lett 88:173120
9. Andrés Vergés M, Mifsud A, Serna CJ (1990) J Chem Soc Farady Trans 86(6):959
10. Sigoli FA, Davolos MR, Jafelicci M (1997) J Alloys Comp 263/263:292
11. Kleinwechter H, Janzen C, Knipping J, Wiggers H, Roth P (2002) J Mater Sci 37:4349
12. Kong YC, Yu DP, Zhang B, Fang W, Feng SQ (2001) Appl Phys Lett 78:407
13. Djurišić AB, Leung YH (2006) Small 2:944